Applying ionic liquids as oil additives for gearboxes: Going beyond the state of the art by bridging the nano-scale and component level

Azhaarudeen ANIFA MOHAMED FARUCK[1,*], **Philipp G. GRÜTZMACHER**[1], **Chia-Jui HSU**[1], **Dominik DWORSCHAK**[2], **Hsiu-Wei CHENG**[2], **Markus VALTINER**[2], **Kristof STAGEL**[3], **Philipp MIKŠOVSKY**[3], **Apurba Ranjan SAHOO**[3], **Aitor SAINZ MARTINEZ**[3], **Katharina BICA-SCHRÖDER**[3], **Michael WEIGAND**[1], **Carsten GACHOT**[1]

[1] *Institut für Konstruktionswissenschaften und Produktentwicklung (IKP), Tribology Research Division, TU Wien, Vienna 1060, Austria*

[2] *Institut für Angewandte Physik (IAP), Applied Interface Physics research group, TU Wien, Vienna 1040, Austria*

[3] *Institut für Angewandte Synthesechemie (IAS), Sustainable Organic Synthesis and Catalysis research group, TU Wien, Vienna 1060, Austria*

Abstract: Ionic liquids (ILs) have been used effectively in many applications for reducing problems related to friction and wear. In this work, the potential of ILs as an anti-wear and extreme pressure lubricant additive for high load-carrying gearbox applications such as helicopter transmissions has been studied. Two halide-free ILs: $P_{8881}(BuO)_2PO_2^-$ (1) and $P_{8881}(MeO)_2PO_2^-$ (2), which are blended at 5 wt% each into a standard non-additivated FVA2 base oil (BO) are examined. Their solid–liquid interface, friction and load-carrying capacity, and wear (scuffing) behavior are studied on the nano-, lab-, and component-scale, respectively, at a different range of temperature and loading conditions by using the atomic force microscopy (AFM), Schwing–Reib–Verschleiß (SRV) friction tests, and Brugger tests, as well as forschungsstelle für zahnräder und getriebebau (FZG) back-to-back gear test rig. The AFM analysis shows nearly no change of adhesion over the full range of studied temperature for the IL blends compared to the BO. Similarly, IL blends demonstrate a very stable coefficient of friction (COF) of around 0.16, which even decreases with increasing test temperatures ranging from 40 to 120 °C. A clear reduction in COF up to 25% is achieved by adding only 5 wt% of the investigated ILs in the BO, and the Brugger tests also show a pronounced enhancement of load-carrying capacity. Finally, on the component-scale, a significant improvement in gear scuffing performance has been observed for both used IL blends. A detailed characterization of the wear tracks from the SRV friction tests via the transmission electron microscopy (TEM) revealed the formation of a phosphate (P–O)-based amorphous tribo-chemical layer of about 20 nm thickness. Therefore, this work may present an approach for ILs to be used as an additive in conventional lubricants due to their ability to enhance the lubrication properties, making them an alternative lubricant solution for high load-carrying gearbox applications.

Keywords: ionic liquids (ILs); additives; gears; scuffing; friction; load-carrying capacity

1 Introduction

Friction and wear in machine elements, such as gears or the piston-cylinder assembly, is a major problem reducing the energy efficiency of these components [1]. Already in Ancient Egypt, lubricants have been used to lower friction and wear by separating the surface sliding in relative motion. To increase the energy efficiency of mechanical components and thus comply with the need for higher sustainability,

---

* Corresponding author: Azhaarudeen ANIFA MOHAMED FARUCK, E-mail: azhaarudeen.faruck@tuwien.ac.at

Nomenclature

Symbol/abbreviation		IL	Ionic liquid
λ	Debye length (nm)	ILb1 and ILb2	Ionic liquid blend 1 and ionic liquid blend 2
AFM	Atomic force microscopy	NMR	Nuclear magnetic resonance
a	Major axis of an elliptical wear scar (mm)	$[P_{8881}]$	Trioctyl(methyl)phosphonium
b	Minor axis of an elliptical wear scar (mm)	$(MeO)_2PO_2^-$	Dimethyl phosphate
B	Brugger load-carrying capacity (N/mm^2)	$(BuO)_2PO_2^-$	Dibutyl phosphate
COF	Coefficient of friction	SEM–EDS	Scanning electron microscopy–energy dispersive X-ray spectroscopy
FTIR	Fourier-transform infrared		
FZG	Forschungsstelle für zahnräder und getriebebau	TEM	Transmission electron microscopy
		TGA	Thermal gravimetry analysis
FFT	Fast Fourier transformation	ZDDP	Zinc dialkyldithiophosphate

researchers worldwide are always searching for new ways to reduce friction and wear. Besides higher energy efficiency, the lifetime of machine elements and thus their safety is also of key significance. One example where this is highly relevant are helicopter gearboxes. In these transmissions, loss of lubrication can occur because of design, maintenance, or operational errors, eventually leading to catastrophic failures. According to aviation standards, the gearbox still has to properly function for at least 30 min after loss of lubrication commences [2, 3].

In the past, great success in enhancing the tribological performance was achieved with the anti-wear (e.g., zinc dialkyldithiophosphate (ZDDP)) and extreme pressure additives (sulphur–phosphorus based), which are still widely used in commercial lubricants. In this context, though ZDDP is well-known as anti-wear additive, its friction reduction mechanism is mainly attributed to an increased load support and based on tribochemical reactions, forming a protective film against corrosion [4]. In many systems, tribochemical reactions (e.g., thermo-oxidative processes) cause the degradation of the lubricant [5]. Moreover, several studies have been focused on the mutual interactions of ZDDP with other additive compounds, e.g., dispersants and detergents, which present in a fully-formulated oil causing rate of decomposition and modification of ZDDP's derived anti-wear film [6–10]. Additionally, new lubrication concepts have been

heavily investigated, and the novel lubricants must also be environmentally friendly and bio-degradable but at the same time economically feasible. Room-temperature ionic liquids (ILs) containing cations (organic) and anions (organic or inorganic) are of great interest as novel lubricants due to their relevance in green chemistry [11–16]. ILs exhibit many unique properties such as low volatility, non-flammability, high thermal stability, high heat capacity and electrical conductivity, and flexible molecular structure, giving them several advantages over classical liquid lubricants and hence making them an attractive alternative for tribological applications [16–19]. However, the two main disadvantages of ILs are that they are quite costly and that their miscibility in base oils (BOs) is often limited [20, 21]. Several research works are indicating that ILs can be used effectively for lubrication of metal alloys and ceramic materials under severe sliding conditions [5, 21–29]. The first study about room-temperature ILs (liquid below 100 °C) was published by Ye et al. [19]. In their study, the authors measured several friction pair combinations and found that the friction performance of the used IL (1-methyl-3-hexylimidazolium tetrafluoroborate) was significantly enhanced compared to the two standard fluorine-containing lubricants (phosphazene and PFPE). The mechanism of the ILs by which they improve the tribological properties has been partially ascribed to the adsorption of the IL onto the surface, where it

forms a layered structure keeping the moving surfaces separated, and especially at higher loads to the tribochemical formation of fluoride tribofilms from the fluorine-containing anions, protecting the metal surface [21]. Inspired by the protective tribofilm formation of ZDDP, phosphate anions were investigated for tribological applications [30], and similar or lower wear than fluorine-based anions could be observed [31, 32]. In terms of the cation, usually longer alkyl chain length results in better lubricity and decrease in friction and wear [21, 33, 34]. Additionally, better wear performance was observed when the cation was functionalized with a phosphate group [35]. Chemical analyses of the wear track by the X-ray photoelectron spectroscopy (XPS) showed that the ILs in the tribo-contact are broken down, resulting from high pressures and partially high temperatures, and then react with the metal surface to form protective tribofilms [36, 37]. In more recent studies, ILs have been used in combination with diamond-like carbon (DLC) coatings [38], new ILs have been tested [20], or the influence of IL concentration and alkyl chain length on the tribological properties have been investigated [39].

Cooper et al. [40] investigated the nanotribological behavior of several ILs on industrially relevant steel surfaces by the atomic force microscopy (AFM) and found an inverse correlation between friction and interfacial structure of the ILs. Cations that had weak interactions with the anions resulted in an easy displacement of the near-surface layers and small lateral forces when compared to the ILs, which showed stronger interactions with the anion. Contradicting this, An et al. [41] demonstrated increasing coefficients of friction (COFs) for decreasing layer thickness in their AFM measurements on mica and graphite. Moreover, Li et al. [42] compared the nanotribological behavior measured by the AFM with the macro-scale performance (ball-on-disc) of ILs as lubricant additives on silica surfaces. They found that the neat IL performs much better than the BO, hexadecane, on both scales, whereas when used as an additive, there are apparent differences between both scales. At the nano-scale, they found good properties for concentrations over 2.0 mol%, but high concentrations are needed on the macro-scale for higher loads.

In general, ILs have been proposed for special applications such as space applications, microelectro-mechanical systems (MEMS), high-temperature environments, machines in clean rooms, or high-pressure applications where friction is high [5, 21]. But they have also successfully been employed in combustion engines where fuel consumption could be significantly decreased compared to the standard SAE30 oil [29]. In some of the special applications, it might be feasible to use ILs as neat lubricants, but for more commercial applications, it would be more beneficial to use them as a lubricant additive to lower the overall costs [21]. In this context, ILs have also shown beneficial performance when used as an additive to BOs [33, 43–45].

Here we study the tribological performance of nano-scale liquid lubricants on different scales, ranging from their nanoscopic behavior with the AFM measurements to an intermedium level with laboratory tribological testing to finally the application level in the form of gears, which are typically applied in helicopter gearboxes. Mainly, the influence of different testing temperatures is investigated with the aim of evaluating the possibility to tailor the IL lubricant to a specific operating temperature in a machine element. In order to minimize the number of variables in the lubricant chemistry, two simple ILs (P8881(BuO)$_2$PO$_2^-$ (1) and P8881(MeO)$_2$PO$_2^-$) (2) were chosen to be used in the BO that contain only one type of additive formulation, which is phosphorous-based such as tricresyl-phosphate (TCP), a well-known anti-wear additive [46, 47]. Moreover, these ILs can be easily produced in large scale in an atom efficient, solvent-, and halide-free synthetic process and show the good miscibility with the BO due to their hydrophobic nature. Additionally, these ILs do not contain halides, fluorine, and chlorine, which can cause corrosion when they are used as lubricants. This would open up a new level of tuning the IL to a particular application, which is one of the main advantages of the "designer fluids".
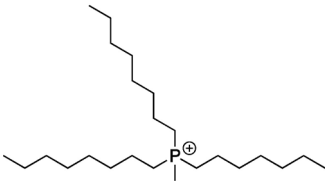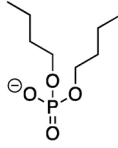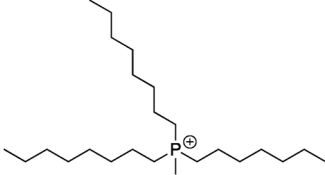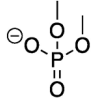
2 Materials, characterization, and testing methods

2.1 Synthesis of ILs and preparation of lubricants

2.1.1 General remarks

Chemicals were purchased from commercial suppliers

Table 1 Molecular name and structure of the two ILs.

IL	Name	Cation	Anion
IL1	Trioctyl(methyl)phosphonium dibutyl phosphate [P$_{8881}$] (BuO)$_2$PO$_2^-$		
IL2	Trioctyl(methyl)phosphonium dimethyl phosphate [P$_{8881}$] (MeO)$_2$PO$_2^-$		

and used without further purification unless otherwise noted.

^{1}H-nuclear magnetic resonance (NMR) and ^{31}P-NMR spectra were recorded from CDCl$_3$ solutions on a NMR spectrometer (Bruker Avance UltraShield 400 (^{1}H: 400 MHz, ^{31}P: 162 MHz)). Chemical shifts are reported in ppm and were calibrated to the residual solvent signal (CDCl$_3$, 1H: 7.26 ppm). Coupling constants are reported in Hertz (Hz). The assignments are based on the comparison with the reported spectra.

The infrared spectra were recorded on a Fourier-transform infrared (FTIR) spectrometer (Perkin Elmer Spectrum 65) equipped with an attenuated total reflectance (ATR) unit (Specac MK II Golden Gate Single Reflection). Karl Fischer titrations were carried out using a semi-automatic, coulometric titrator (Mitsubishi CA-21 Moisture Meter). For measurements, an aliquot of 1 g of IL was stored under air, and measurements were performed after 1 min, 1 h, and 24 h.

The results from ^{1}H-NMR and ^{31}P-NMR (Figs. S1–S4), FTIR (Figs. S5 and S6), and Karl Fischer titrations (Table S1) for the amount of water content in neat ILs can be found in the Electronic Supplementary Material (ESM).

2.1.2 Synthesis of ILs

The ILs (Table 1) were synthesized according to a modified literature protocol in a halide-free manner [48].

1) [P$_{8881}$] (MeO)$_2$PO$_2^-$ (2)

Freshly-distilled trioctylphosphine (1.0 equiv.) was transferred to a round-bottom flask under an argon atmosphere. Trimethyl phosphate (1.2 equiv.) was added to the flask meanwhile stirring. The temperature was increased stepwise to 140 °C, and the mixture was stirred under an inert atmosphere for 72 h. After completion of the reaction, the excess trimethyl phosphate was removed under vacuum (0.2 mbar, 95 °C). The desired product ([P$_{8881}$] (MeO)$_2$PO$_2^-$) (2) was obtained as orange, viscous liquid in 98% yield.

^{1}H NMR (400 MHz, CDCl$_3$) δ 3.64–3.48 (m, 6H, 2x CH$_3$OP), 2.33 (ddt, J = 13.5, 10.0, 3.1 Hz, 6H, 3x PCH$_2$(CH$_2$)$_6$CH$_3$), 2.10–1.97 (m, 3H, PCH$_3$), 1.72–1.13 (m, 36H, 3x PCH$_2$(CH$_2$)$_6$CH$_3$), 0.94–0.77 (m, 9H, 3x P(CH$_2$)$_7$CH$_3$). ^{31}P NMR (162 MHz, CDCl$_3$) δ 31.99 (cation), 2.24 (anion). IR (cm^{-1}): 2,955, 2,855, 1,532, 1,250, and 1,053. Water content (ppm): 465 (1 min), 2,106 (60 min), and 8,406 (24 h).

2) [P$_{8881}$] (BuO)$_2$PO$_2^-$ (1)

A round-bottom flask was charged with ([P$_{8881}$] (MeO)$_2$PO$_2^-$) (2) (1.0 equiv.) and (BuO)$_2$PO$_2^-$ (1.2 equiv.) under an argon atmosphere. Triethylamine (1.4 equiv.) was added dropwise meanwhile cooling with an ice bath. After the addition was complete, the reaction mixture was stirred for 20 min at 0 °C and overnight at room temperature. Distilled water was then added to the mixture, and it was stirred vigorously for 16 h at room temperature. The mixture was transferred in a separatory funnel and washed once with a mixture of triethylamine and distilled water (10:90 *V/V*) and 4 times with distilled water. Finally, the residual water was removed under vacuum

(0.2 mbar, 95 °C). The desired IL [P_{8881}] (BuO)$_2$PO$_2^-$ (1) was obtained as slightly yellowish, viscous liquid with a yield of 97%.

^{1}H NMR (400 MHz, CDCl$_3$) δ 3.80 (td, *J* = 6.8 and 5.8 Hz, 4H, 2*x* CH$_3$(CH$_2$)$_2$CH$_2$OP), 2.35 (ddt, *J* = 13.5, 9.8, and 5.2 Hz, 6H, 3*x* PCH$_2$(CH$_2$)$_6$CH$_3$), 2.04 (d, *J* = 13.6 Hz, 3H, PCH$_3$), 1.69–1.12 (m, 44H, 3*x* PCH$_2$(CH$_2$)$_6$CH$_3$, 2*x* CH$_3$(CH$_2$)$_2$CH$_2$OP), 0.86 (q, *J* = 7.2 Hz, 15H, 3*x* P(CH$_2$)$_7$CH$_3$, 2*x* CH$_3$(CH$_2$)$_3$OP). ^{31}P NMR (162 MHz, CDCl$_3$) δ 32.05 (cation), 0.58 (anion). IR (cm^{-1}): 2,926, 2,856, 1,465, 1,243, and 1,071. Water content (ppm): 606 (1 min), 1,434 (60 min), and 16,743 (24 h).

2.1.3 *Formulation of blends*

After synthesis, two mixtures were prepared by adding each IL discretely to the standard FVA2 BO as additives with a concentration of 5 wt% each. The BO is a highly-refined mineral oil composed of paraffin (62%) and naphthene (35%) and is free from any additive packages before adding the respective IL. Due to their design featuring long alkyl chains, the ILs used in this work are miscible at 5 wt% in the BO used. To improve miscibility, the IL blends (ILb1 and ILb2) were additionally mechanically stirred for about 2 h at room temperature before the start of the tribological experiments. Westerholt et al. [48] have demonstrated very promising tribological properties of such phosphonium-based ILs as additives at 5 wt% in BO (mineral) that showed better miscibility. This is analogous to the stated hypothesis that the long chain hydrocarbons in the IL structure renders the IL more lipophilic due to the increase of apolar domains, thereby improving the compatibility with neutral oil molecules [49]. Other research groups also found that long aliphatic substituents on the IL ions (cation and/or anion) lead to suitable solubility in BOs [50–52].

2.2 Lubricant characterization

2.2.1 *Viscosity*

Kinematic viscosities of the BO and IL blends (ILb1 and ILb2) are determined using a viscometer (Anton Paar Stabinger SVM 3000) according to ASTM D 7042 [53] standard at 40 and 100 °C (Table 2).

2.2.2 *Thermal stability and wettability*

Thermal stability of the neat ILs were determined by conducting the thermogravimetric analysis (TGA) using a TGA analyzers (TA Instruments Q500). About 15 µg of BO, neat ILs, and IL blends are heated up to 500 °C with increasing heating step of 5 °C/min under air atmosphere.

Contact angles of the BO and IL blends on the polished bearing steel (100Cr6) surface are determined using a contact angle measurement device (Krüss DSA-30). The used material is the same as for the friction tests on the ball-on-disc tribometer. A droplet of 2.5 µL was applied onto the sample surface from a pipette (Eppendorf). To measure the contact angle at equilibrium conditions of the sessile droplet, the measurement was done after 30 s. The contact angles were recorded at three different temperatures of 40, 90, and 120 °C. At least, three droplets were measured at each temperature.

2.2.3 *Lubricant interface analysis by the AFM*

The temperature-dependent adhesion force measurements were performed with an Environmental AFM (Asylum Research Cypher ES) with the AFM software ver. 16 (Asylum Research). The cantilevers used were ContGB-G contact mode cantilevers (BudgetSensor) with a typical spring constant of 0.2 N/m. Temperature variation experiments were performed under feedback control of the system with an accuracy of 0.1 °C.

Table 2 Blend concentrations and viscosities of the BO and IL blends.

Lubricant	Notation	Blend concentration (wt%)	Viscosity of BO and IL blends (cSt)	
			40 °C	100 °C
FVA2	BO	0	31.0	5.24
FVA2 + [P_{8881}] (BuO)$_2$PO$_2^-$	ILb1	5	33.0	5.72
FVA2 + [P_{8881}] (MeO)$_2$PO$_2^-$	ILb2	5	32.6	5.43

Iron thin film substrates with a thickness of ~40 nm on mica were produced with a home-built magnetron sputtering system. The iron sputtering target with a purity of 99.99% was purchased from Kurt J. Lesker Company representing the steel that was used for the study (> 80% iron). For achieving low roughness, V1 optical grade and atomically smooth muscovite [0001] mica sheets were used as the supporting substrate for iron thin film. Mica sheets were freshly cleaved shortly before introduction into the sputtering chamber.

Under a given controlled temperature, 100 force–distance (F–D) measurements were evenly measured over an area of 1 μm × 1 μm with a 0.5 Hz of probing frequency. The acquired deflection-Z piezo position curves were properly calibrated with deflection sensitivity and the measured spring constant using thermal noise method for generating F–D isotherms. At least 50 F–D curves are randomly selected for analyzing probability densities of the F–D characteristics (heat mappings).

2.3 Tribometrical experiments

2.3.1 Ball-on-disc tribometer

Friction measurements were carried out using a ball-on-disc tribometer, a Schwing–Reib–Verschleiß (SRV) tribometer (Optimol Instruments, Prüftechnik GmbH) under pure sliding conditions. The ball (diameter: 10 mm) and disc (diameter: 25 mm, thickness: 8 mm) specimens are made of bearing steel (100Cr6). Both substrate and counter-body are polished to a roughness value (R_a) of 0.3 and 0.1 μm, respectively, and have a hardness value of 60 HRC. Prior to the tests, specimens were cleaned with toluene and petroleum ether each for 10 min using an ultrasonic bath and dried in normal air. The ball is pressed and oscillated against a static disc with a constant speed and load. The experiments are performed at three different temperatures, 40, 90, and 120 °C. Before starting the friction experiments, two droplets (0.1 mL) of BO and IL blends are applied onto the substrate. Table 3 summarizes the parameters of the conducted friction experiments. The COF is recorded throughout the experiment.

2.3.2 Brugger lubricant tester

Boundary lubrication behavior can be studied by

Table 3 Ball-on-disc (SRV tribometer) test parameters.

Test condition	
Load (GPa)	1.5
Speed	0.12 m/s or 15 Hz
Test duration (min)	60 (432 m in distance)
Stroke length (mm)	4
Temperature (°C)	40, 90, and 120

using a standardized Brugger tribometer that provides information on the load-carrying capacity of the lubricating oil according to the standard DIN 51347 [54] under pure sliding conditions and at room temperature. Before establishing the contact, the test lubricant is poured onto the ring surface, ensuring that the oil covers the entire surface of the ring by gravity. Then, a constant load F_N of 400 N is applied by a cylinder positioned normal to a rotatable ring surface and at right angles (Fig. 1). The ring rotates with a constant speed of 960 r/min for 30 s, producing a defined elliptical wear scar, as shown in Fig. 1. The laser scanning confocal microscope (Keyence VK-X1000 3D) is used to determine the stretch of major *a* and minor *b* axis lengths (in the *XY* direction) of the elliptical wear scar, which is proportional to the load-carrying capacity of the tested lubricants. Equation (1) is used to calculate the Brugger load-carrying capacity *B* of each lubricating oil examined. At least, three repetitions are carried out under the same test conditions to arrive an average load-carrying
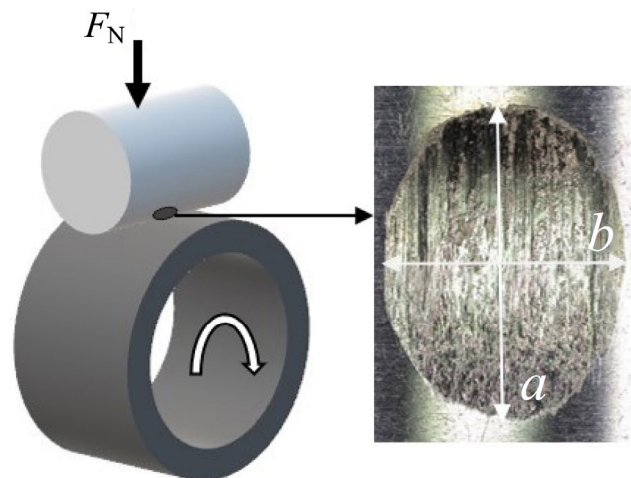

Fig. 1 Schematic representations of the contact configuration of the Brugger tribometer (left) and an elliptical wear scar (on cylinder) indicating the major and minor axes *a* and *b* (right).

capacity value for each lubricating oil.

$$B = \frac{4F_N}{ab\pi} \left(\text{N} / \text{mm}^2 \right) \tag{1}$$

2.3.3 Gear testing

The forschungsstelle für zahnräder und getriebebau (FZG) back-to-back gear test rig is used for conducting the standard gear scuffing tests at Vienna University of Technology (TU Wien), Vienna, Austria, according to DIN 51354, FZG (A/8.3/90) [55]. Case carburized, 16MnCr6 (A-type) gear pair (wheel and pinion) with a center distance of 91.5 mm, the peripheral speed of 8.3 m/s, and oil temperature of 90 °C are loaded against each other using a clutch plate to apply the desired torque load. In this method, the gears are subjected to 12 increasing load steps of Hertzian stresses, each tested for 15 min. After each step, the gear flanks are visually inspected for scuffing marks until reaching a critical load step, where the cumulative scuffing marks from all the pinion teeth exceed the width of a single tooth. The test gears were cleaned with special benzine before conducting the scuffing tests. The material data and the detailed testing conditions are given in the standard [55]. To investigate the influence of temperature on the performance of the IL blends, the gear testing was conducted at 40 °C (lower) and 120 °C (higher) temperatures from standard operating temperature of 90 °C. Since the FZG back-to-back test gear rig has provided a very reliable results in the standard conditions as well as in our previous work [2], the scuffing tests were limited to one test for the lower and higher operating temperature conditions. However, the standard gear scuffing tests with oil temperature at 90 °C are conducted twice using both side of a gear pair. Additionally, the load steps were also increased from the maximum standard load step of 12 to 14 for the higher-temperature (120 °C) scuffing tests in order to subject the IL blends to much severe loads to determine their extended performance that can further reveal the extreme pressure additive property of the ILs.

2.4 Topographical and chemical characterization of the wear marks

The wear marks from the friction tests were investigated in terms of their morphology and possible tribofilm formation using the following different surface characterization methods. Topography and load bearing capacity (for the Brugger tester) were analysed using a laser scanning confocal microscope (Keyence VK-X1000 3D). A more detailed analysis of the topography as well as a characterisation of the tribofilm composition was performed via the scanning electron microscope (SEM; Quanta FEG 250, Thermo Fisher Scientific) equipped with an energy-dispersive X-ray spectroscopy (EDS) system (Octane Elite, EDAX) and Raman spectroscope (Jobin Yvon Horiba, HR800). Finally, nano-structural properties of the tribofilm were investigated using the field emission transmission electron microscope (TEM; FEI TECNAI F20) operated at 200 kV and equipped with a high brightness X-FEG cathode.

3 Results

3.1 Thermal stability and wettability

The TGA provides information about the decomposition temperatures of BO, neat ILs, and IL blends by measuring changes in weight with increasing temperature of the system, as shown in Fig. 2(a). The onset of decomposition temperature for neat ILs starts roughly at 200 °C. The neat ILs (IL1 and IL2) behave identical up to a temperature of 275 °C. Then a two-step decomposition behavior is observed, which is a little stronger for IL1 with the anion containing the di-butyl group, leading to a greater weight loss. The decomposition of the BO and IL blends starts roughly at 175 °C. For the IL blends, the effect in terms of thermal stability is not evident anymore, as they behave nearly identical to the BO.

One of the factors that determines the ability of a lubricating oil to form a stable oil film on a steel surface is its contact angle. Contact angles less than 45° indicate that the liquid is highly hydrophilic [56]. In this work, the contact angles measured are below 30°, indicating that the BO and IL blends are providing good wettability on the given steel surface. As can be seen from Fig. 2(b) and Fig. S7 in the ESM, the contact angles of the BO decrease continuously from 25° to 3° with increasing temperatures. In combination with a reduction in viscosity for increasing temperature,
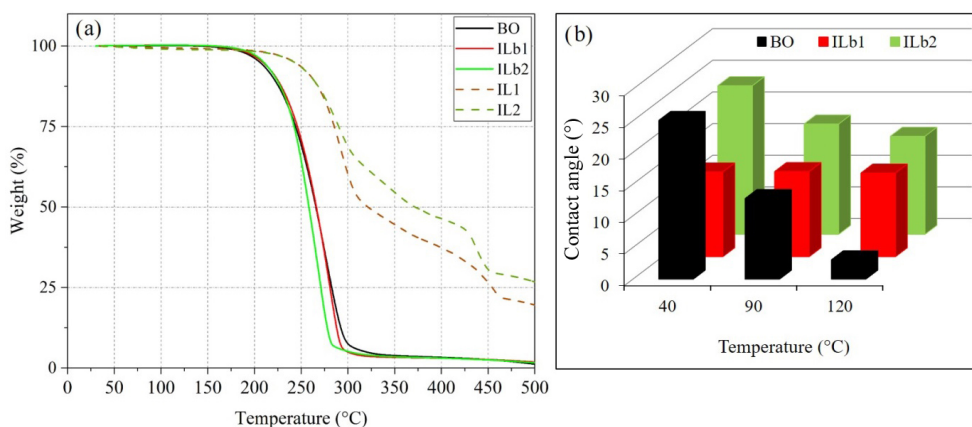
Fig. 2 (a) Thermogravimetric behaviors of neat ILs, BO, and IL blends and (b) contact angles of BO and IL blends on bearing steel (100Cr6).

this could lead to thinner oil films and more severe solid–solid contact scenarios, therefore resulting in higher friction and wear. Adding only 5 wt% of the respective IL into the BO significantly increases the stability of the contact angle when measured at different temperatures. At 40 °C, the contact angle of ILb2 is around 23° and therefore slightly lower than that of the BO but does not decrease as strongly as that of the BO with increasing temperatures, recording the lowest contact angle of 14.6° at 120 °C. The contact angle of ILb1 remains unaffected by temperature and the values of around 13° are recorded for all temperatures. When comparing the wettability of the two IL blends, the contact angle of ILb1 is generally lower than that of ILb2, indicating a stronger tendency for spreading on the surface. In general, the stability of the wetting properties of the IL blends indicates that the tribological properties of surfaces lubricated with these IL blends are less affected by varying wetting properties when measured at different temperatures.

3.2 Lubricant interface characterization by the AFM

The lubrication property of the system is often dominated by interaction forces and molecular interfacial layering of lubricant molecules at the solid/liquid interface. To probe interaction profiles and interfacial structuring, we utilized the contact mode AFM to measure the F–D characteristics of the system.

Figure 3 shows the temperature-dependent AFM F–D profiles and measured adhesion between a gold-coated tip and a smooth iron thin film sputtered onto a mica substrate (~40 nm thick) in BO and ILb1. In detail, Fig. 3(a) exemplarily shows the representative F–D curves during approach and retraction in BO as a function of the temperature. The insets (top right) in Fig. 3(a) show a statistical comparison of BO and ILb1 force vs. distance characteristics during approach with more than 50 measured AFM F–D curves that are overlaid in a heat plot for each lubricant. In the BO, the approach curves indicate a strong attractive force, which increased with increasing temperature from 25 °C up to 120 °C. Equally, also the range of the attractive force increases significantly with the increasing temperature. In contrast, ILb1 with 5 wt% of IL1 in BO exhibits a temperature-independent low adhesion, further showing repulsive characteristic, indicative of interfacial ion adsorption and no long-range attraction. The repulsive profile indicates no substantial layering, but an exponentially increasing repulsion is an indication of a disordered ion layer at the interface in ILb1. Comparing both data sets suggests that the long-range component in the BO is a result of a long-range electrostatic interaction due to surface charging, which is not screened effectively in the BO. In contrast, in ILb1 the surface charging is effectively screened by ion adsorption at the interface.

Figure 3(b) further summarizes the adhesion force distribution over a range of studied temperatures as measured during the separation of the contacting surfaces. The plotted adhesive minima are calculated from the difference between the minimum value before
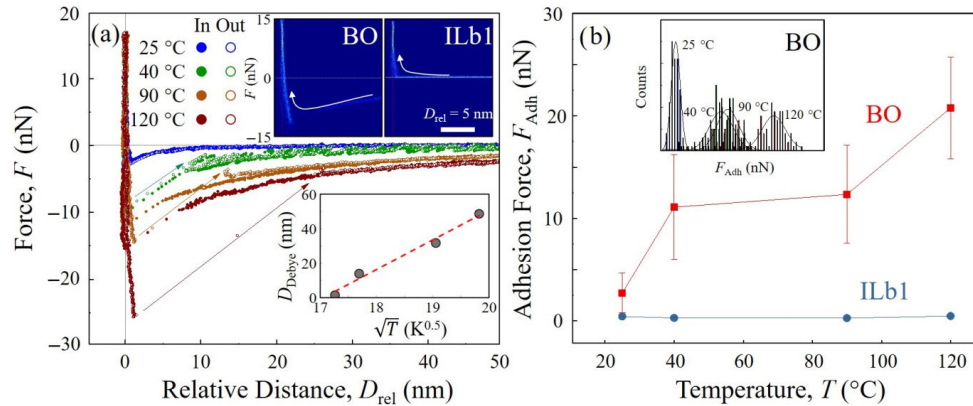
Fig. 3 Comparison of the AFM F–D characteristics of BO and ILb1 between a gold-coated AFM cantilever and a smooth iron thin film sputtered on mica under controlled temperatures. (a) Representative AFM F–D approach (solid circle) and retraction (hollow circle) curves of BO at 25, 40, 90, and 120 °C. The insets (top right) show the probability mappings (> 50 curves) of the F–D profile of BO and ILb1 at 90 °C (operating temperature). (b) Adhesion force between the tip and iron surface with the presence of BO and ILb1 under tested temperatures. The inset shows an example histogram of the measured adhesive events from BO, where the distributions were fitted using normal Gaussian function.

separation and the base line at $F = 0$. The average and error bars of measured adhesion forces (> 50 effective measurements) of BO (red) and ILb1 (blue) under a controlled temperature are extracted as the full with at half maximum (FWHM) from the Gaussian distribution of the adhesion. The data further confirm a significant increase of the adhesion in BO at 40 °C. The data from 40 to 90 °C indicated a plateau with shallow increase, followed by a drastic increase again from 90 to 120 °C. In line with the approach data, ILb1 (5 wt% IL1) shows nearly no change of adhesion force over the full range of studied temperature.

To further understand the physics of the change of interaction profile, it is interesting to inspect the temperature-dependent distance shift of the long-range attractive profile, as shown in Fig. 3(a). Specifically, the long-range profile could be fitted well with an electric double layer interaction using the DLVO theory, where the characteristic decay distance (Debye length λ) is defined as

$$\lambda = \sqrt{\frac{\varepsilon_r \varepsilon_0 k_B T}{2 N_A e^2 I}} \tag{2}$$

where ε_r and ε_0 are the permeability of the solution and vacuum, respectively; k_B is the Boltzmann constant; T is the temperature; N_A is the Avogadro's number; e is the charge of electron; and I is the ionic strength of the solution.

As shown in the inset (bottom right) in Fig. 3(a), the fitted temperature depended on the change of λ shows good linear proportionality of $R^2 = 0.97$ with the square root of temperature ($\sqrt{T}$), which confirms their physical correlation. This demonstrates that the observed interaction is governed by electric double layer properties and ineffectively screened surface charging in the BO. In the BO system, with the absence of ions in the solution, I is extremely small, leading to a significant contribution of long-range electrostatic forces. As soon as ions (ILs) are added, I shortens λ and lowers the surface charge by direct adsorption of ions to the interface, resulting in a significant screening of the interaction forces. Also, the lower adhesion, i.e., effective repulsions, are in line with an adsorption of the ions onto the surfaces. Specifically, the ion adsorption results in a contact situation with ions between the surfaces. This lowers the van der Waals interactions as well as the charge interactions in IL containing BO.

3.3 Tribometry

3.3.1 *Friction behavior of the IL blends measured by the SRV tribometer*

Figure 4 shows the optical images of the wear scars formed after conducting the friction tests on the SRV tribometer with BO, ILb1, and ILb2 at 40, 90, and 120 °C. It is evident that for all the measurements
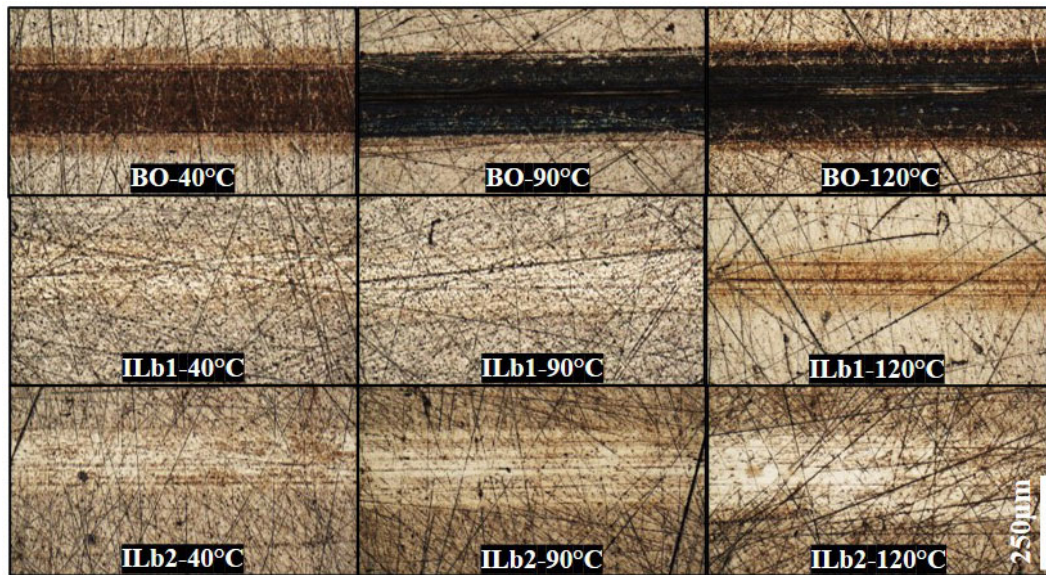
Fig. 4 Optical images of the wear tracks from sliding friction tests conducted for BO, ILb1, and ILb2 at 40, 90, and 120 °C.

performed with BO, a dark layer remains on the substrate, likely to be a reaction product of the decomposed BO compounds (carbonaceous residues). The width of the wear track increases, and the colour of the dark layer intensifies as the test temperature increases. In contrast, after testing the IL blends, such a dark layer is not observed, even though the wear track on the substrate tested with ILb1 shows a brownish colour. It is worth mentioning that despite the clear modification of the surfaces as a consequence of tribological testing, in particular for the cases where BO was used, almost no material is removed. The frictional results of the SRV tests are summarised in Fig. 5. At 40 °C, BO has recorded the lowest COF with values close to 0.14 at the end of the test. However, a pronounced increase in COF is observed when the test temperature increases to 90 and 120 °C, recording higher COF of slightly above 0.18 (Figs. 5(b) and 5(c)). In contrast, both ILb1 and ILb2 show similar and constant COFs for different test temperatures, even slightly decreasing from around 0.16 at 40 °C to around 0.14 for 120 °C. Additionally, no or a shorter running in phase under given test conditions are observed for the tests performed with the IL blends, which is particularly true for the measurements at 120 °C. Figure 5(d) represents the average COF values calculated from three different tests (after 10 min of running-in) for all the three

lubricating oils at 40, 90 and 120 °C. Here, IL blends show roughly 12% decrease in average COF with the increase in temperature from 40 to 120 °C, but BO shows 20% increase.

3.3.2   Load-carrying capacity of the IL blends by the Brugger test rig

The Brugger test results provide a standardized tribometrical evaluation on the load-carrying capacity of the lubricating oils operating under boundary lubrication. An increased average load-carrying capacity of 10% and 25% compared to BO is demonstrated for ILb1 and ILb2, respectively (Fig. 6). The increase in average load-carrying capacity shows that the ILs tend to improve the anti-wear property of the BO under boundary lubrication. When comparing the two IL blends, ILb2 containing di-methyl phosphate anion shows a better performance than the ILb1 with di-butyl anion. Also, from Fig. 6, the average load-carrying capacity of ILb2 is about 25 N/mm², which is in the range of fully-formulated and commercially-used turbine oils as determined on the same test setup from the author's previous work [2].

3.3.3   Gear scuffing behavior of the IL blends by FZG

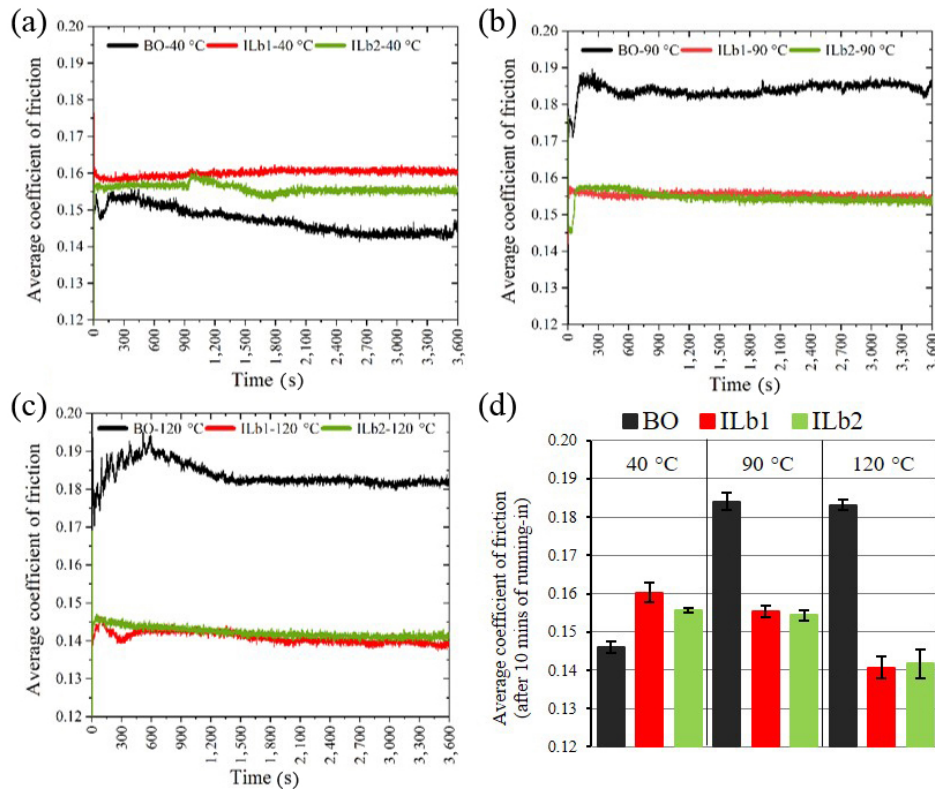Gear scuffing tests on a standard FZG test rig were performed to evaluate the suitability of the ILs to be

Fig. 5 Evolution of COF from each liquid at (a) 40 °C, (b) 90 °C, and (c) 120 °C. (d) Average values of the COFs calculated from three different tests.
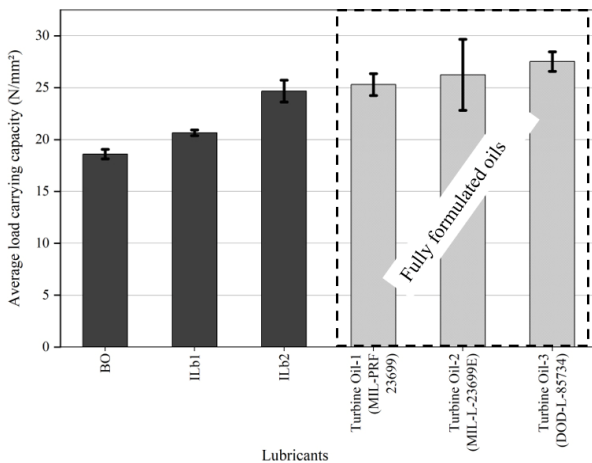

Fig. 6 Average load-carrying capacities of BO, ILb1, and ILb2; also, of the fully-formulated commercial turbine oils used in helicopter applications determined by a standard Brugger tester according to DIN 51347-1.

Fig. 7 FZG scuffing test results showing load-carrying capacities of the BO and ILbs in terms of load-levels tested at 40, 90, and 120 °C, and the arrows indicate the scuffing load capacities beyond load-level 12. Scuffing load-level results for fully-formulated and commercially-used aviation turbine oil (TO) and engine oil (EO) tested at 90 °C are presented on the right.

used in a real application. Figure 7 shows the average scuffing performance of the IL blends compared to BO. In this work, the maximum scuffing load-level is increased from 12 to 14 at the testing temperature of 120 °C to push the IL blend ILb2 to its limits in terms of temperature and load.

The results from the FZG experiments show that the gears lubricated with BO failed relatively early at load-levels of 3–5, reaching a maximum critical load-level of 5 at 120 °C. The tests performed with

ILb1 show a substantial improvement with a maximum average load-level of 8.5 at standard operating conditions (90 °C). Most notably, ILb2 tremendously improves the BO characteristics and has out-performed (> 12) BO and ILb1 at all the tested temperature with zero scuffing marks at load-level 12, thus qualifying as a high anti-scuffing lubricating oil. Increasing the load-level to above 12, however, leads to severe scuffing marks at 120 °C on the gears lubricated with ILb2, thus reaching its full load-carrying capacity at the load-level 13. A scuffing load-level of more than 12 is typically achieved by fully-formulated turbine oil (TO) and engine oil (EO) oils investigated on the same test setup in the author's previous work [2] (Fig. 7). This emphasises the outstanding performance of ILb2 and shows that scuffing prevention mainly depends on either sufficient fluid film lubrication or surface-binding additives compounds.

3.4 Surface characterization after friction tests

To investigate possible modifications of the surfaces induced by tribological testing, the chemical and microstructural states of the wear tracks were characterized by the Raman spectroscopy, SEM/EDS, and TEM.

3.4.1 Tribo-chemical analysis using the Raman spectroscopy

The wear tracks of the substrates tested with the SRV experiments were examined by the Raman spectroscopy, and the results are presented in Fig. 8(a). In general, all the wear tracks reveal no evidence of the tribofilm formation as the Raman shift shows mainly iron oxide signals. The resonance of iron oxide (Fe_3O_4) and carbon-based products (D and G peaks) were observed at the wavelength of 660, 1,350, and 1,580 cm^{-1}, respectively [57, 58]. However, no notable difference was identified between wear tracks of different lubricants from the general examinations. Therefore, a more detailed study focusing on specific regions inside the wear tracks was conducted, and significantly different spectra were recorded. In Fig. 8(b), two points (A and B) in the wear track of ILb2 at 90 °C were examined separately. Point A is appearing in dark brown in the optical image of the wear track, and its spectrum shows peaks
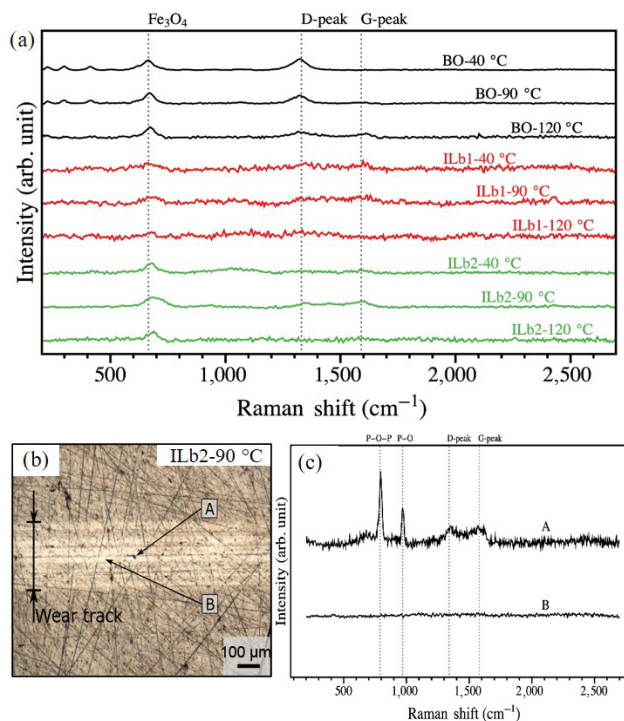

Fig. 8 (a) Raman spectra of the wear tracks after SRV testing with BO, ILb1, and ILb2 under three different operating temperatures, (b) optical micrograph of the wear track of ILb2 at 90 °C after the SRV test, and (c) Raman spectra of Positions A and B on the wear track.

corresponding to phosphorus- and carbon-related bonding. The D and G peaks of carbon were found at 1,358 and 1,576 cm^{-1}, respectively. Two other maxima were found at 792 and 974 cm^{-1} with the FWHMs of 26.3 and 26.2 cm^{-1}, respectively. The peak at 792 cm^{-1} can be assigned to the symmetric stretching of P–O–P bond, whereas 974 cm^{-1} was attributed to the symmetric stretching of P–O bond [59–61]. As a comparison, no peak can be found at Point B outside the dark region, which seems as a clean surface with metallic luster.

3.4.2 Tribo-chemical analysis using the SEM/EDS

The SRV test wear tracks are further investigated using the SEM equipped with EDS to determine the surface chemical composition in an attempt to find more evidences of tribo-layer formation. For this, the wear tracks from the SRV friction tests conducted at 120 °C lubricant temperature were chosen as they demonstrate the lowest COF. Figure 9 reveals clear wear marks for the measurements conducted with BO. In contrast, the surface for the measurements with ILb1
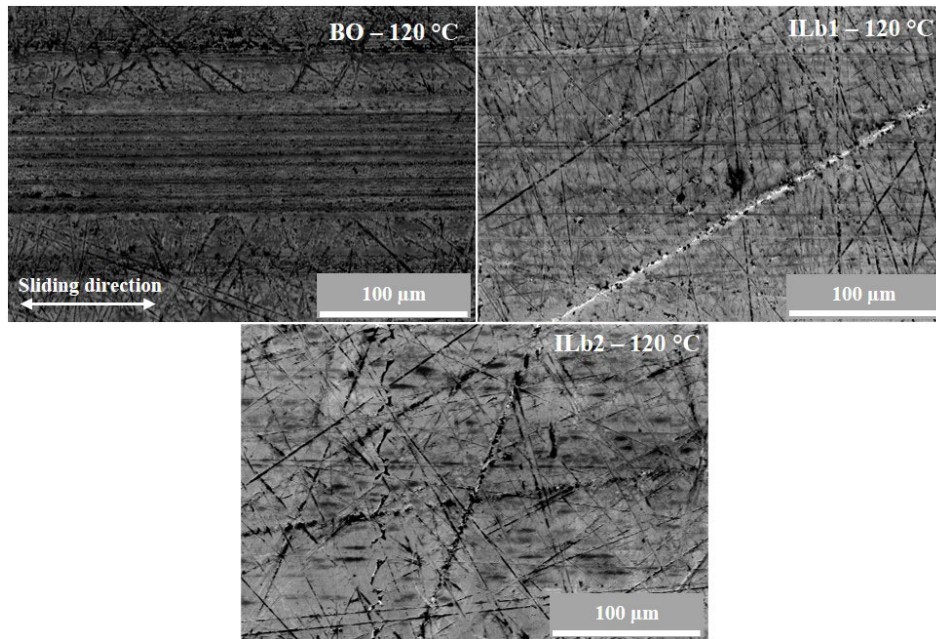
Fig. 9 SEM images of the SRV test wear track of BO, ILb1, and ILb2 at 120 °C.

is smoother and shows much less but still visible wear marks for the measurements with ILb1. The grooves in sliding direction are indicating abrasive wear as the acting wear mechanism. On the contrary, for the surface tested with ILb2, no wear marks can be found, and the scratching marks from metallographic preparation of the sample can still be observed. These findings are in accordance to the optical images of the wear tracks in Fig. 4. This implies that a more resilient boundary film must be formed at the material interface, thus preventing from wear. The EDS spectra from these SRV friction test wear tracks are shown in Fig. 10. In addition to iron, carbon, and oxygen peaks, the wear tracks produced with the IL blends (ILb1 and ILb2) show phosphorous peaks nearly at 2 keV, indicating a tribofilm induced by ILs in BO. It is worth mentioning that the phosphorus signal is much stronger for ILb2.

3.4.3 Tribo-film analysis using the TEM

To investigate the tribofilm formation in more detail, a TEM lamella was prepared from the wear track of the substrate measured via SRV testing with ILb2 at 90 °C. Figure 11(a) shows an overview TEM image of the wear track's cross-section (left) and a high-magnification TEM image as well as a fast Fourier transformation (FFT) pattern of the tribofilm (right).

The formed tribofilm is composed of a single layer with a thickness in the range of 10 to 20 nm. The FFT analysis reveals that the diffraction pattern of the tribofilm is made up of an amorphous structure. From Fig. 11(b), the EDS elemental mapping of the test surface lubricated with ILb2 reveals that the tribofilm is mainly composed of phosphates (P–O) (Fig. 11(b)). However, this single layer structure is not representing the entire tribofilm formed due to the small sample area, therefore not excluding other possible mixtures containing iron phosphates and oxides, as observed with the Raman spectroscopy.
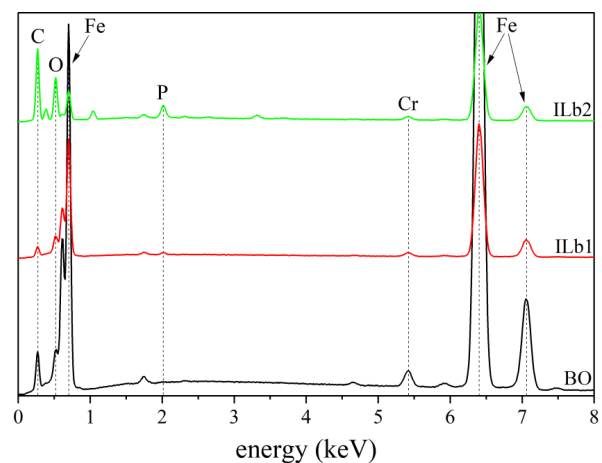

Fig. 10 EDS spectra with elemental (at%) characterized from inside the friction test wear track of BO, ILb1, and ILb2 at 120 °C.
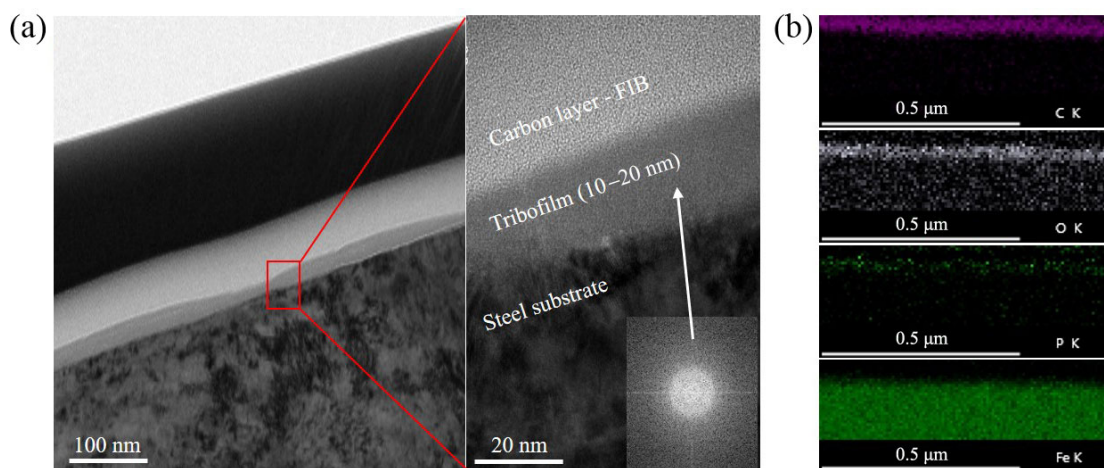
Fig. 11 (a) TEM micrographs and electron diffraction pattern (bottom right) and (b) EDS elemental mappings of the tribofilm on the SRV disc surface lubricated with ILb2 at 90 °C.

4   Discussion

Thermal analysis via the TGA demonstrated that the ILs are stable up to temperatures far above the application temperature, and that the decomposition temperature of the BO is not affected by adding the ILs. Adding only 5 wt% of ILs (IL1 and IL2) to an unformulated BO significantly improves the interaction and friction and wear characteristics of the BO, which was shown on the nano- and laboratory scale as well as in gears under realistic conditions representing the component level.

On the nano-scale (AFM), a clear dependence of test temperature could be observed. The AFM measurements showed increasing adhesion with increasing temperature for the BO, whereas the adhesion of the IL blends is constant over a temperature range of 25–120 °C (Fig. 3). This shows that the ILs perform well at all temperatures, while the BO indicates an increasing adhesion. Hence, when adding ILs into the BO, the strong adhesion at high temperature can be effectively reduced, resulting in a considerably improved friction and wear performance of the system also at elevated temperatures.

The laboratory-scale (SRV) measurements are also in accordance with the nano-scale findings, where the COF is significantly increasing with higher temperature when BO is used, but is constant or even slightly decreasing in the case of IL blends. This could be connected to the change in wetting properties when adding ILs to the BO. Higher temperatures lead to a stronger spreading of the BO over the surface, which can, in combination with a decreasing viscosity, result in a thinner lubricant film, leading to the change of the respective tribological regime [62] and therefore potentially more solid–solid contact accompanied with higher friction and wear [63]. In contrast to that, the wetting properties of the IL blends are much more stable over the applied temperatures, thus contributing to a stable tribological performance at higher temperatures. Additionally, tribochemical reaction of the IL's interfacial ions (cations and anions) is a major factor improving their lubricating performance. This can be related to the research on the structural influence of cations and anions on lubricity. Cations with longer alkyl chains corresponds to a tighter adsorption on sliding surfaces, providing better lubrication properties of ILs [64] as well as preventing direct surface–surface contact which in turn reduces the friction [43, 64–66]. The mechanism in which density-packed adsorption of lubricant molecules on the sliding surfaces is essential is also referred as the Bowden–Tabor model [67]. But this is contradictory in case of anions where longer alkyl chain lengths typically lead to an increase in the COF. This was demonstrated in a work by Kawada et al. [68], who analyzed the tribo-chemical reactions of sulphate and phosphate anion-based ILs and showed that during the reaction, outgassing of the cation components and alkoxide of the anions enable the sulfate and phosphate to remain on the solid surface, thus forming the friction reducing tribofilm. In this process, sulphate

and phosphate anion-based ILs with shorter alkyl-chain lengths react more easily with the sliding surface to form the tribofilm, which enhances the lubrication performance. This behavior is evident in the SRV frictional results from Fig. 5. Despite no significant differences in frictional performance between the two ILs, the surface lubricated with ILb1 is showing signs of increased wear or tribochemical reactions for the highest temperature of 120 °C, where the system is stressed the most (Figs. 4 and 10). The quite similar friction behavior might be induced by identical cations of both ILs, whereas an effective tribofilm formation preventing wear is more prominent for ILb2, having the anion with shorter (di-methyl) alkyl-chain. This shorter chain length of alkyl-chain facilitates tribofilm formation, and thus effectively protects the surface. This is confirmed by the chemical analyses via the SEM– and TEM–EDS, which show a pronounced single-layer protective tribofilm composed of amorphous phosphate (P–O) compounds. The findings in terms of the wear behavior are also confirmed by the Brugger test as well, where much higher loads than that during the SRV testing are applied. These tests show a clear trend in terms of load-carrying capacity (i.e., wear), with the specimens lubricated with BO performing the worst, ILb1 demonstrating intermediate values, and ILb2 performing the best (Fig. 6). This again indicates a more effective tribofilm formation of ILb2, triggered by the anion with the shorter alkyl-chain length.

The component-scale (FZG) gear tests and the Brugger tests involve higher loads, therefore, it is not surprising that the same trend is observed in both cases. The gears lubricated with BO are performing the worst, and the gears lubricated with ILb2 (shorter anion alkyl chain) are performing the best in terms of scuffing wear (Fig. 7). Interestingly, in contrast to the laboratory test on the SRV setup, no clear trend in terms of temperature dependence could be observed for FZG testing. This can be correlated with the way that the lubricant is finally guided to the contact area in the different setups. During FZG testing, the most severe contact happens under fully lubricated conditions. Therefore, wetting properties are not as important as for SRV testing, where a finite volume (0.1 mL) of oil is dropped onto the surface before starting the test.

Chemical analysis of the wear tracks from SRV testing demonstrated the formation of a beneficial tribolayer for the surfaces lubricated with IL blends, consisting of a single protective layer formed by phosphate (P–O) compounds. Studies also reported that the presence of P and O chemical signals on steel surfaces mostly form iron phosphate $Fe(PO_4)$ and other oxidic reaction layers [31, 43, 69]. It can be assumed that this tribolayer helps to prevent direct contact between the two contacting/sliding surfaces, thus greatly increasing the anti-wear property of the BO. As the applied contact pressures in SRV testing and FZG measurements are similar, it is highly likely that this tribolayer formation also takes place during FZG testing, therefore boosting the critical load-level for scuffing. It is known that a certain activation energy is necessary for tribolayer formation to occur [70]. This might be the reason for a reduction in friction with increasing temperature during SRV testing, as tribolayer formation will be facilitated at higher temperatures. It is also necessary to point out that the tribolayer formed by lubricating with $[P_{8881}]\,(MeO)_2PO_2^-$ IL blend is comparable to the tribolayers formed by fully-formulated oils investigated in author's previous work in terms of reacting with steel surface, as both are phosphate-based, forming iron oxide and iron phosphate bindings [2]. Also, the lubrication mechanism of conventional lubricant additives such as ZDDP and TCP is similar to this observed here, as these form phosphate-rich boundary layers [31, 71, 72]. Therefore, the ILs investigated in this study, in particular $[P_{8881}]\,(MeO)_2PO_2^-$, could be a potential alternative to well-known anti-wear and extreme pressure additives used in commercial automotive and aviation gearbox applications.

5　Conclusions

This study systematically implements a combination of test procedures from nano-scale to component-scale to investigate the tribological performance of two halide-free phosphonium based ILs ($[P_{8881}]\,(BuO)_2PO_2^-$ and $[P_{8881}]\,(MeO)_2PO_2^-$) as lubricant additives in FVA2 BO. The main conclusions are as follows:

The negligible adhesive force between the gold coated tip and iron surface determined by the AFM measurements shows that both the ILs alter the

interfacial interactions of the BO. This also partially affects the wetting behavior of the blended BO on the steel substrate.

A strong dependance of temperature is observed for the BO with increasing COF when the temperature increases from 40 to 90 and 120 °C during SRV testing. Contradicting to BO, a stable and slightly decreasing COF is observed with respect to the IL blends. However, by overstressing the tribosystem with both mechanical and thermal energy, the IL blend (ILb1) containing longer alkyl-chain length anion (($(BuO)_2PO_2^-$) shows increased wear behavior.

Extensive chemical/microstructural characterization by the Raman, SEM–EDS, and TEM demonstrated signs of tribofilm formation on the surfaces lubricated with IL blended BO, which is stronger for ILb2. In particular, TEM results revealed a 10–20 nm thick single-layered amorphous tribofilm, mainly consisting of iron phosphates and oxides on the SRV worn surface lubricated with 5 wt% of ILb2 ($[P_{8881}]$ $(MeO)_2PO_2^-$) in BO. ILb2 containing the anion with shorter alkyl-chain length is assumed to lead to an enhanced tribofilm formation due to an easier reaction with the substrate surface, thus more effectively protecting the surface.

High contact pressure tribo-testing using the Brugger tester and FZG gear test rig reveals a more distinguishing difference between the two IL blends in terms of anti-wear, scuffing, and load-carrying capacity. Such experiments are also typically carried for investigating the extreme pressure property of gear lubricating oils. The results from both of these tests are in correlation with each other, representing better tribological performance in the order as follows: ILb2 > ILb1 > BO.

These ILs can be a promising alternative for the conventional extreme pressure additives mainly due to their anti-scuffing performance in gear tests. In combination with these ILs, varying concentrations and blending with a fully-formulated oil may deliver interesting tribological characteristics.

Acknowledgements

Electronic Supplementary Material Supplementary material is available in the online version of this article at https://doi.org/10.1007/s40544-022-0650-5.

References

[1]   Rosenkranz A, Grützmacher P G, Gachot C, Costa H L. Surface texturing in machine elements—A critical discussion

for rolling and sliding contacts. *Adv Eng Mater* **21**(8): 1900194 (2019)

[2]   Mohamed Faruck A A, Hsu C J, Doerr N, Weigand M, Gachot C. How lubricant formulations and properties influence the performance of rotorcraft transmissions under loss of lubrication conditions. *Tribol Int* **151**: 106390 (2020)

[3]   Transportation Safety Board of Canada. Main gearbox malfunction/collision with water. Investigation Report A09A0016: Cougar Helicopters Inc. Sikorsky S-92A, C-GZCH. 180, 2010.

[4]   Gachot C, Hsu C, Suárez S, Grützmacher P, Rosenkranz A, Stratmann A, Jacobs G. Microstructural and chemical characterization of the tribolayer formation in highly loaded cylindrical roller thrust bearings. *Lubricants* **4**(2): 19 (2016)

[5]   Minami I. Ionic liquids in tribology. *Molecules* **14**(6): 2286–2305 (2009)

[6]   Kasrai M, Fuller M S, Bancroft G M, Ryason P R. X-ray absorption study of the effect of calcium sulfonate on antiwear film formation generated from neutral and basic ZDDPs: Part 1—Phosphorus species. *Tribol Trans* **46**(4): 534–542 (2003)

[7]   Kapsa P, Martin J M, Blanc C, Georges J M. Antiwear mechanism of ZDDP in the presence of calcium sulfonate detergent. *J Lub Tech* **103**(4): 486–494 (1981)

[8]   Rounds F G. Additive interactions and their effect on the performance of a zinc dialkyl dithiophosphate. *ASLE Trans* **21**(2): 91–101 (1978)

[9]   Inoue K, Watanabe H. Interactions of engine oil additives. *ASLE Trans* **26**(2): 189–199 (1983)

[10]   Wu Y L, Dacre B. Effects of lubricant-additives on the kinetics and mechanisms of ZDDP adsorption on steel surfaces. *Tribol Int* **30**(6): 445–453 (1997)

[11]   Welton T. Room-temperature ionic liquids. Solvents for synthesis and catalysis. *Chem Rev* **99**(8): 2071–2084 (1999)

[12]   Omotowa B A, Phillips B S, Zabinski J S, Shreeve J M. Phosphazene-based ionic liquids: Synthesis, temperature-dependent viscosity, and effect as additives in water lubrication of silicon nitride ceramics. *Inorg Chem* **43**(17): 5466–5471 (2004)

[13]   Jin C M, Ye C F, Phillips B S, Zabinski J S, Liu X Q, Liu W M, Shreeve J M. Polyethylene glycol functionalized dicationic ionic liquids with alkyl or polyfluoroalkyl substituents as high temperature lubricants. *J Mater Chem* **16**(16): 1529–1535 (2006)

[14]   Palacio M, Bhushan B. Ultrathin wear-resistant ionic liquid films for novel MEMS/NEMS applications. *Adv Mater* **20**(6): 1194–1198 (2008)

[15]   Yu G Q, Zhou F, Liu W M, Liang Y M, Yan S Q. Preparation of functional ionic liquids and tribological investigation of their ultra-thin films. *Wear* **260**(9–10): 1076–1080 (2006)

[16]   Aviles M D, Saurin N, Espinosa T, Sanes J, Arias-Pardilla J, Carrion F J, Bermudez M D. Self-lubricating, wear resistant protic ionic liquid-epoxy resin. *Express Polym Lett* **11**(3): 219–229 (2017)

[17]   Fan M J, Song Z H, Liang Y M, Zhou F, Liu W M. *In situ* formed ionic liquids in synthetic esters for significantly improved lubrication. *ACS Appl Mater Interfaces* **4**(12): 6683–6689 (2012)

[18]   Saurín N, Minami I, Sanes J, Bermúdez M D. Study of the effect of tribo-materials and surface finish on the lubricant performance of new halogen-free room temperature ionic liquids. *Appl Surf Sci* **366**: 464–474 (2016)

[19]   Ye C F, Liu W M, Chen Y X, Yu L G. Room-temperature ionic liquids: A novel versatile lubricant. *Chem Commun* (21): 2244–2245 (2001)

[20]   Zhu L L, Zhao Q, Wu X H, Zhao G Q, Wang X B. A novel phosphate ionic liquid plays dual role in synthetic ester oil: From synthetic catalyst to anti-wear additive. *Tribol Int* **97**: 192–199 (2016)

[21]   Somers A E, Howlett P C, MacFarlane D R, Forsyth M. A review of ionic liquid lubricants. *Lubricants* **1**(1): 3–21 (2013)

[22]   Torimoto T, Tsuda T, Okazaki K I, Kuwabata S. New frontiers in materials science opened by ionic liquids. *Adv Mater* **22**(11): 1196–1221 (2010)

[23]   Zhang S G, Zhang Q H, Zhang Y, Chen Z J, Watanabe M, Deng Y Q. Beyond solvents and electrolytes: Ionic liquids-based advanced functional materials. *Prog Mater Sci* **77**: 80–124 (2016)

[24]   Bermúdez M D, Jiménez A E, Sanes J, Carrión F J. Ionic liquids as advanced lubricant fluids. *Molecules* **14**(8): 2888–2908 (2009)

[25]   Palacio M, Bhushan B. A review of ionic liquids for green molecular lubrication in nanotechnology. *Tribol Lett* **40**(2): 247–268 (2010)

[26]   Bermúdez M D. Introduction to the ionic liquids special issue. *Tribol Lett* **40**(2): 213 (2010)

[27]   Dörr N. Special issue on ionic liquids as lubricants. *Proc Inst Mech Eng Part J J Eng Tribol* **226**(11): 889–890 (2012)

[28]   Austen Angell C, Ansari Y, Zhao Z F. Ionic liquids: Past, present and future. *Faraday Discuss* **154**(0): 9–27 (2012)

[29]   Predel T, Pohrer B, Schlücker E. Ionic liquids as alternative lubricants for special applications. *Chem Eng Technol* **33**(1): 132–136 (2010)

[30]   VHuang G W, Yu Q L, Ma Z F, Cai M R, Zhou F, Liu W M. Oil-soluble ionic liquids as antiwear and extreme pressure additives in poly-α-olefin for steel/steel contacts. *Friction* **7**(1): 18–31 (2019)

[31] Minami I, Inada T, Sasaki R, Nanao H. Tribo-chemistry of phosphonium-derived ionic liquids. *Tribol Lett* **40**(2): 225–235 (2010)

[32] Somers A E, Biddulph S M, Howlett P C, Sun J Z, MacFarlane D R, Forsyth M. A comparison of phosphorus and fluorine containing IL lubricants for steel on aluminium. *Phys Chem Chem Phys* **14**(22): 8224–8231 (2012)

[33] Jiménez A E, Bermúdez M D. Imidazolium ionic liquids as additives of the synthetic ester propylene glycol dioleate in aluminium–steel lubrication. *Wear* **265**(5–6): 787–798 (2008)

[34] He Y Q, Li H, Qu C Y, Cao W, Ma M. Recent understanding of solid–liquid friction in ionic liquids. *Green Chem Eng* **2**(2): 145–157 (2021)

[35] Mu Z G, Zhou F, Zhang S X, Liang Y M, Liu W M. Effect of the functional groups in ionic liquid molecules on the friction and wear behavior of aluminum alloy in lubricated aluminum-on-steel contact. *Tribol Int* **38**(8): 725–731 (2005)

[36] Liu W M, Ye C F, Gong Q Y, Wang H Z, Wang P. Tribological performance of room-temperature ionic liquids as lubricant. *Tribol Lett* **13**(2): 81–85 (2002)

[37] Wang H Z, Lu Q M, Ye C F, Liu W M, Cui Z J. Friction and wear behaviors of ionic liquid of alkylimidazolium hexafluorophosphates as lubricants for steel/steel contact. *Wear* **256**(1–2): 44–48 (2004)

[38] Arshad M S, Kovač J, Cruz S, Kalin M. Physicochemical and tribological characterizations of WDLC coatings and ionic-liquid lubricant additives: Potential candidates for low friction under boundary-lubrication conditions. *Tribol Int* **151**: 106482 (2020)

[39] Pejaković V, Tomastik C, Dörr N, Kalin M. Influence of concentration and anion alkyl chain length on tribological properties of imidazolium sulfate ionic liquids as additives to glycerol in steel–steel contact lubrication. *Tribol Int* **97**: 234–243 (2016)

[40] Cooper P K, Wear C J, Li H, Atkin R. Ionic liquid lubrication of stainless steel: Friction is inversely correlated with interfacial liquid nanostructure. *ACS Sustain Chem Eng* **5**(12): 11737–11743 (2017)

[41] An R, Qiu X H, Shah F U, Riehemann K, Fuchs H. Controlling the nanoscale friction by layered ionic liquid films. *Phys Chem Chem Phys* **22**(26): 14941–14952 (2020)

[42] Li H, Somers A E, Howlett P C, Rutland M W, Forsyth M, Atkin R. Addition of low concentrations of an ionic liquid to a base oil reduces friction over multiple length scales: A combined nano- and macrotribology investigation. *Phys Chem Chem Phys* **18**(9): 6541–6547 (2016)

[43] Barnhill W C, Qu J, Luo H M, Meyer H M III, Ma C, Chi M F, Papke B L. Phosphonium-organophosphate ionic liquids as lubricant additives: Effects of cation structure on physicochemical and tribological characteristics. *ACS Appl Mater Interfaces* **6**(24): 22585–22593 (2014)

[44] Barnhill W C, Luo H M, Meyer III H M, Ma C, Chi M F, Papke B L, Qu J. Tertiary and quaternary ammonium-phosphate ionic liquids as lubricant additives. *Tribol Lett* **63**(2): 22 (2016)

[45] Zhou Y, Qu J. Ionic liquids as lubricant additives: A review. *ACS Appl Mater Interfaces* **9**(4): 3209–3222 (2017)

[46] Bartz W J, Krüger V. Influence of lubricants on the pitting fatigue of gears. *Wear* **35**(2): 315–329 (1975)

[47] Ghose H M, Ferrante J, Honecy F C. The effect of tricresyl-phosphate (TCP) as an additive on wear of iron (Fe). NASA Technical Memorandum, 1987.

[48] Westerholt A, Weschta M, Bösmann A, Tremmel S, Korth Y, Wolf M, Schlücker E, Wehrum N, Lennert A, Uerdingen M, et al. Halide-free synthesis and tribological performance of oil-miscible ammonium and phosphonium-based ionic liquids. *ACS Sustain Chem Eng* **3**(5): 797–808 (2015)

[49] Yu B, Bansal D G, Qu J, Sun X Q, Luo H M, Dai S, Blau P J, Bunting B G, Mordukhovich G, Smolenski D J. Oil-miscible and non-corrosive phosphonium-based ionic liquids as candidate lubricant additives. *Wear* **289**: 58–64 (2012)

[50] Qu J, Luo H M, Chi M F, Ma C, Blau P J, Dai S, Viola M B. Comparison of an oil-miscible ionic liquid and ZDDP as a lubricant anti-wear additive. *Tribol Int* **71**: 88–97 (2014)

[51] Qu J, Truhan J J, Dai S, Luo H, Blau P J. Ionic liquids with ammonium cations as lubricants or additives. *Tribol Lett* **22**(3): 207–214 (2006)

[52] Elsentriecy H H, Luo H M, Meyer H M, Grado L L, Qu J. Effects of pretreatment and process temperature of a conversion coating produced by an aprotic ammonium-phosphate ionic liquid on magnesium corrosion protection. *Electrochimica Acta* **123**: 58–65 (2014)

[53] ASTM D7042. Standard test method for measuring dynamic viscosity of liquids using a Stabinger Viscometer (incl. the calculation of kinematic viscosity). ASTM, 2013.

[54] DIN 51347-2. Testing of lubricants—Testing under boundary lubricating conditions with the Brugger lubricant tester—Part 2: General working principles. DIN, 2000.

[55] DIN ISO 14635-1. FZG-prüfverfahren A/8,3/90 zur bestimmung der fresstragfähigkeit von schmierölen. DIN, 2006. (in German)

[56] Borruto A, Crivellone G, Marani F. Influence of surface wettability on friction and wear tests. *Wear* **222**(1): 57–65 (1998)

[57] De Faria D L A, Venâncio Silva S, de Oliveira M T. Raman microspectroscopy of some iron oxides and oxyhydroxides. *J Raman Spectrosc* **28**(11): 873–878 (1997)

[58] Childres I, Jauregui L A, Park W, Cao H L, Chen Y P. Raman spectroscopy of graphene and related Materials. In: *New Developments in Photon and Materials Research*. Jang J I, Ed. Nova Science Publishers, 2013: 403–418.

[59] Gauvin M, Dassenoy F, Minfray C, Martin J M, Montagnac G, Reynard B. Zinc phosphate chain length study under high hydrostatic pressure by Raman spectroscopy. *J Appl Phys* **101**(6): 063505 (2007)

[60] Berkani S, Dassenoy F, Minfray C, Martin J M, Cardon H, Montagnac G, Reynard B. Structural changes in tribo-stressed zinc polyphosphates. *Tribol Lett* **51**(3): 489–498 (2013)

[61] Andrushchenko V, Benda L, Páv O, Dračínský M, Bouř P. Vibrational properties of the phosphate group investigated by molecular dynamics and density functional theory. *J Phys Chem B* **119**(33): 10682–10692 (2015)

[62] Stribeck R. Die wesentlichen eigenschaften der gleit- und rollenlager. *Zeitschrift Des Vereines Deutscher Ingenieure* **36**: 1341–1348 (1902) (in German)

[63] Park S, Cho Y, Sung K, Han N. The effect of viscosity and friction modifier on fuel economy and the relationship between fuel economy and friction. *SAE Int J Fuels Lubr* **2**(2): 72–80 (2010)

[64] Gusain R, Bakshi P S, Panda S, Sharma O P, Gardas R, Khatri O P. Physicochemical and tribophysical properties of

trioctylalkylammonium bis(salicylato)borate (N888n-BScB) ionic liquids: Effect of alkyl chain length. *Phys Chem Chem Phys* **19**(9): 6433–6442 (2017)

[65] Amorim P M, Ferraria A M, Colaço R, Branco L C, Saramago B. Imidazolium-based ionic liquids used as additives in the nanolubrication of silicon surfaces. *Beilstein J Nanotechnol* **8**: 1961–1971 (2017)

[66] Li H, Rutland M W, Atkin R. Ionic liquid lubrication: Influence of ion structure, surface potential and sliding velocity. *Phys Chem Chem Phys* **15**(35): 14616–14623 (2013)

[67] Bowden F P, Tabor D. The friction and lubrication of solids Part II. *Physics Today* **17**: 72 (1964)

[68] Kawada S, Watanabe S, Tadokoro C, Sasaki S. Effects of alkyl chain length of sulfate and phosphate anion-based ionic liquids on tribochemical reactions. *Tribol Lett* **66**(1): 8 (2018)

[69] Zhang L, Feng D P, Xu B. Tribological characteristics of alkylimidazolium diethyl phosphates ionic liquids as lubricants for steel–steel contact. *Tribol Lett* **34**(2): 95–101 (2009)

[70] Spikes H. The history and mechanisms of ZDDP. *Tribol Lett* **17**(3): 469–489 (2004)

[71] Battez A H, Bartolomé M, Blanco D, Viesca J L, Fernández-González A, González R. Phosphonium cation-based ionic liquids as neat lubricants: Physicochemical and tribological performance. *Tribol Int* **95**: 118–131 (2016)

[72] Martin J M. Antiwear mechanisms of zinc dithiophosphate: A chemical hardness approach. *Tribol Lett* **6**(1): 1–8 (1999)

Azhaarudeen ANIFA MOHAMED FARUCK. He is currently working as a project assistant at Vienna University of Technology (TU Wien), Austria and since 2017 he is pursuing his Ph.D. studies on the topic of loss of lubrication in Helicopter gearbox. He was working as Junior Scientist at AC2T research GmbH, from 2014 till 2020 performing research activities focused on surface contacts and lubrication. He has a great interest in experimental research in lubrication, solid lubricant coatings, surface texturing, and friction & wear characterization.

Philipp G. GRÜTZMACHER. He joined the tribology group at TU Wien in late 2019. Before, he was active in the field of tribology at the Institute of Functional Materials, Saarland University, Germany, led by Prof. Dr. Frank MÜCKLICH, where he obtained his Ph.D. degree for the tribological investigation of multi-scale surface textures in October 2019. His current research interests focus on the tribological mechanisms of 2D materials, the near-surface microstructural development of metals during sliding as well as surface texturing and surface engineering. He has authored more than 35 papers in highly ranked peer-reviewed journals. In 2021 he joined the early career editorial board of *Tribology Letters* and in 2022 the editorial board of *Tribology - Materials, Surfaces & Interfaces*.
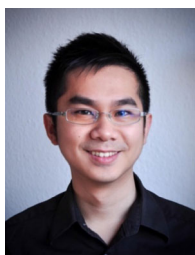
Chia-Jui HSU. He is a material scientist doing research on surface engineering and tribology. He has a background in mechanical engineering and obtained his Ph.D. degree in material science and engineering from Saarland University, Germany, in 2022. His current research focuses on developing industrial PVD/ALD methods for functional thin film deposition. Moreover, microstructural and chemical characterization are also his expertise.

Hsiu-Wei CHENG. He received his Ph.D. degree in chemistry and biochemistry from Ruhr University Bochum in association with Max-Plank Institute for Iron Research, Germany, in 2017. He later worked as University Assistant in TU Wien, Austria, from 2017 till 2021. Starting from August 2021, he became Assistant Professor in the Department of Chemistry, "National" Taiwan University, till now. His research interests are focused in electrochemistry-driven interfacial processes, ranging from corrosion, catalysis to battery charging and reaction in bio interphase.
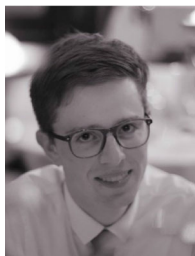
Dominik DWORSCHAK. He received his M.S. degree in chemistry from Freiberg University of Mining and Technology, Germany, in 2017. In 2021 he received his Ph.D. degree in interface science from TU Wien, Austria, with focus on atomic force microscopy. Now he is a team leader with the Helmholtz-Institute Erlangen-Nürnberg for Renewable Energies, Germany. His research areas cover electrochemical interfaces, electrocatalysis, and automation.

Philipp MIKŠOVSKY. He currently conducts his Ph.D. studies in the research group of Prof. Katharina SCHRÖDER at TU Wien in the field of sustainable organic chemistry and catalysis. He focuses on the valorization of carbon dioxide representing a cheap and abundant raw material using ionic liquids as catalysts. He received his master's degree in 2019 (at TU Wien) working in the field of synthetic organic chemistry focusing on medicinal chemistry and photopharmacology. Furthermore, he is interested in continuous flow chemistry, supercritical CO_2 conversions and extractions, and the utilization of bioderived feedstocks.

Kristof STAGEL. He finished his B.Sc. studies at the University of Pannonia, Hungary, in 2017. Thereafter, he studied as a pharmaceutical engineer at the Budapest University of Technology, Hungary. He joined the SCHRÖDER research group as a Ph.D. candidate in January 2020, and his research mainly focuses on the halide-free continuous synthesis of hydrophobic ionic liquids and their catalytic application.

Aitor SAINZ MARTINEZ. He received his Bachelor degree in chemistry in 2014 and his master degree in synthetic and industrial chemistry in 2015 at University of the Basque Country, Spain. Then, he was a Ph.D. student in the Laboratory of Sustainable Organic Synthesis and Catalysis, TUWien. Currently, he is about to finalize his Ph.D. degree, meanwhile he is working a as a Product and Validation Specialist at Intervet GesmbH (MSD) in the animal health field.

Apurba Ranjan SAHOO. He received his Ph.D. degree in organic chemistry from University of Rennes 1, France, in 2017. He joined the Sustainable Organic Synthesis and Catalysis Research Group at TU Wien, Austria, as a postdoctoral fellow in 2018. His research interests include organic synthesis and catalysis. He is currently appointed as an associate specialist at MSD GesmbH, Austria.

Carsten GACHOT. He received his Ph.D. degree from Saarland University, Germany, in 2012, where he studied the effects of laser interference patterning on the microstructure and topography of metallic surfaces with a focus on tribological applications under Prof. Dr. Frank MÜCKLICH and Prof. Dr. Martin H. MÜSER. For this work, he was awarded by the European Honda initiation grant in 2011. He was an academic visitor at the Tribology Group at the Imperial College London, UK, and is currently the head of the Tribology Research Group at TU Wien, Austria. Additionally, Prof. GACHOT is a visiting professor at the Pontifical Catholic University in Santiago de Chile and chief editor of the peer reviewed journal *Industrial Lubrication and Tribology* of the Emerald Publishing Group Leeds UK.

Katharina BICA-SCHRÖDER. She received her Ph.D. degree in technical chemistry from TU Wien, Austria. She later accepted a position as research fellow at QUILL in Belfast, UK working with leading experts in the field of green chemistry. After returning to TU Wien in October 2009 for a tenured position, she established a new research group focused on sustainable chemistry. She was promoted to full professor for sustainable chemistry in 2020 and received an ERC Consolidator Grant 2019. Her research interests are based on sustainable organic chemistry, with a special focus on: (i) novel catalytic processes for asymmetric synthesis, (ii) carbon capture and valorization techniques (CCU), particularly on photocatalytic CO_2 activation, and (iii) the recovery of valuable ingredients from industrial waste streams using advanced fluid technologies.

Markus VALTINER. He finished his Ph.D. degree at the Max-Planck-Institute für Eisenforschung GmbH, Germany, in 2008, where he worked on dissolution mechanism of oxides in aqueous environments and on binding mechanism of organic molecules to oxide surfaces using atomic force microscopy, XPS and SIMS. As a postdoc, he moved to the Department for Chemical Engineering at the University of California, Santa Barbara (UCSB), USA and worked in the group of J. N. ISRAELACHVILI. At UCSB his work focused on developing and using the electrochemical surface forces apparatus. Afterwards he returned to Germany and continued this work from 2012 until 2016 as group leader at the Max-Planck-Institute für Eisenforschung, and from 2016 until 2017 as Professor for colloid and interface chemistry at the Freiberg University of Technology, Germany. In 2017 he joined the Department of Physics, TU Wien, Austria, as faculty member and since 2020 he is also acting scientific head of the Center for Electrochemistry and Surface Technology GmbH in Wiener Neustadt, Austria.

Michael WEIGAND. He is a professor at TU Wien, Austria, since 2008. His expertise is machine design, helicopter transmissions, rehabilitation engineering, and is an organizer of the working group aviation at TU Wien. He received his Ph.D. degree from Technical University Darmstadt, Germany, in 1990. He represents Austria in International Forum for Aviation Research (IFAR), leading the IFAR-Initiative "Vertical Lift" in which 15 nations discuss future rotorcraft applications.